PHYSICAL REVIEW C VOLUME 48, NUMBER 5 NOVEMBER 1993

Coupled-channel potential for nucleons and deltas

J. Haidenbauer
Institut für Theoretische Physik, Universität Graz, A-8010 Graz, Austria

K. Holinde
Institut für Kernphysik der Kernforschungsanlage, D-5100 Jülich, Germany

Mikkel B. Johnson
Los Alamos National Laboratory, Los Alamos, New Mexico 87545
(Received 3 May 1993)

We propose a nucleon-nucleon potential for which the NN, $N\Delta$, and $\Delta\Delta$ channels are coupled by energy-independent, nonlocal interactions constructed from meson-exchange interactions. The same vertex couplings that were utilized in earlier studies based on the Bonn single-channel NN potential are adopted. We arrive at our interaction by applying an extension of the folded diagram expansion to coupled channels. The coupled-channel formalism facilitates studies of the interplay between nucleon and delta degrees of freedom and bound-state properties of nuclear matter and finite nuclei. It also establishes a framework that might simplify the treatment of nucleon-nucleon scattering to energies above pion-production threshold.

PACS number(s): 12.40.Qq, 13.75.Cs, 21.60.−n, 24.10.Eq

I. INTRODUCTION

Previously we constructed a theoretical nucleon-nucleon potential suitable for investigating bound-state properties of nuclear matter and nuclei based on the folded-diagram expansion [1]. The use of folded diagrams permits one to obtain an energy-independent potential, for which the computational problem of evaluating the many-body theory is simplified compared to the case of energy-dependent interactions. Furthermore, many-body theory using folded diagrams is streamlined in the sense that fewer diagrams appear to be required and a tendency for some corrections to cancel can be seen [2]. The reproduction of the nucleon-nucleon (NN) phase shifts in Ref. [1] is comparable to that obtained using the full Bonn potential [3] at low energy (below $E_{\rm lab} \approx 150$ MeV), but at the higher energies we find some differences that we believe are related to the proximity to the nucleon-delta ($N\Delta$) threshold, where the folded-diagram expansion will begin to break down.

In this paper we want to extend our folded-diagram approach by introducing coupled channels involving the Δ isobar. In such an alternative formulation of the many-body problem the Δ degrees of freedom are put on an equal footing with nucleons. This is advantageous because (1) the Δ plays an important role in nuclei, and (2) Faddeev formulations of few-body systems are naturally generalized to handle the Δ degrees of freedom. It thus paves the way for examining the importance of the Δ-nucleon interaction on bound-state properties of nuclei and nuclear matter. In addition the energy dependence associated with the $N\Delta$ [and delta-delta ($\Delta\Delta$)] channels is handled exactly when the relativistic Schrödinger equation is solved. Therefore, the discrepancies found in Ref. [1] for some phase shifts should now be reduced, which turns out indeed to be the case.

The paper is organized as follows. In Sec. II we explain the folded-diagram expansion for the coupled-channel potentials, and in Sec. III we show the numerical results. Finally in Sec. IV we present our conclusions.

II. FOLDED-DIAGRAM EXPANSION

The method of folded diagrams as applied to the NN potential is described in detail in Ref. [4]. There, the Δ states were considered as "passive" degrees of freedom, meaning that they did not occur as dynamical variables of the interaction. The folded-diagram interaction was calculated (perturbatively) in terms of "boxes," which are pieces of Feynman diagrams for which the propagators for the passive states (mesons are also passive) are internal lines. The lines entering and leaving the box are always "active" lines, meaning that they are associated with degrees of freedom that appear explicitly in the equations of motion. The goal of folded diagrams is to define the effective instantaneous (but nonlocal) potential appropriate to the model space (i.e., corresponding to a particular selection of active and passive degrees of freedom), expressed as an expansion in terms of boxes. The idea leading to the instantaneous potential is to integrate out all the time variables of the box save one, which is the time at which the potential acts. The details are straightforward but somewhat involved, and the interested reader may refer to the original papers for a systematic development of the theory.

Here, as opposed to Ref. [4], the Δ lines are to be considered as included among the set of active degrees of freedom. Whereas, in Ref. [4] we had only an NN potential, we now have an $N\Delta$ and $\Delta\Delta$ potential as well as transition potentials among NN, $N\Delta$, and $\Delta\Delta$ states.

We begin our study with the off-diagonal potentials $NN \to N\Delta$, $NN \to \Delta\Delta$, and $N\Delta \to \Delta\Delta$, turning next to the diagonal potentials.

A. Transition potentials

We will treat the off-diagonal or transition potentials to leading order, i.e., only through one-meson exchange. The one-meson-exchange boxes corresponding to the transition potentials are shown in Figs. 1(a), 1(b), and 1(c) for the cases $NN \leftrightarrow N\Delta$, $NN \leftrightarrow \Delta\Delta$, and $N\Delta \leftrightarrow \Delta\Delta$, respectively. The corresponding folded diagrams are shown in Fig. 2. The horizontal dashed line is the time at which the potential acts relative to the time of absorption and emission. Note that this time is chosen differently for the cases in Figs. 2(a) and 2(c), where the two particles in the initial or final states are not of the same mass, compared to Fig. 2(b), where the two particles have the same mass in both the initial state and in the final state. It turns out that for Figs. 2(a) and 2(c), the only choice of time base that avoids a singular potential is to place it at the vertex, where the baryon mass change occurs. There is more freedom to place the time base in Fig. 2(b), and the choice of the midpoint in time between emission and absorption can be shown to simplify the structure of the expansion in higher orders of perturbation theory.

The denominator structure for the terms in Figs. 2(a)–2(c) can be read off from Eq. (19) of Ref. [4]. We find for the case of $NN \leftrightarrow N\Delta$ corresponding to $\lambda = -1$ of that equation ($\mathbf{q} \equiv \mathbf{p} - \mathbf{p}'$)

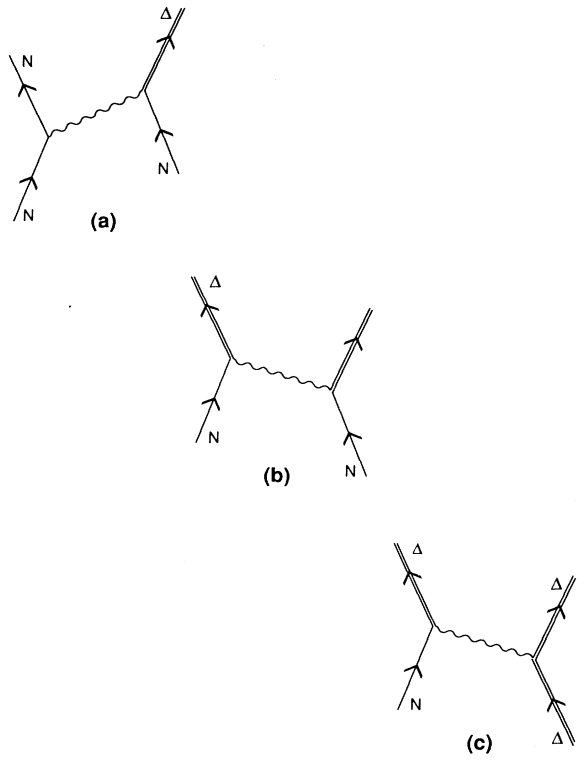

FIG. 1. One-meson-exchange boxes contributing to the transition potentials $NN \to N\Delta$, $NN \to \Delta\Delta$, and $N\Delta \to \Delta\Delta$.

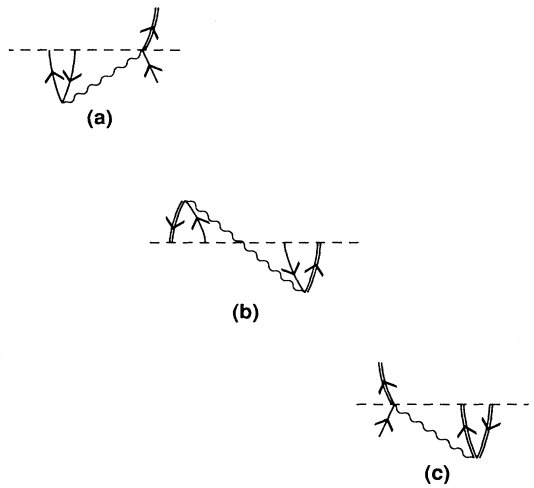

FIG. 2. One-meson-exchange folded diagrams for the transition potentials $NN \to N\Delta$ (a), $NN \leftrightarrow \Delta\Delta$ (b), and $N\Delta \leftrightarrow \Delta\Delta$ (c).

$$\frac{1}{[\sqrt{p^2+m_N^2}-\sqrt{p'^2+m_N^2}]^2-q^2-\mu^2}\,, \tag{2.1}$$

and for $NN \leftrightarrow \Delta\Delta(\lambda=0)$

$$\frac{1}{-q^2-\mu^2}\,, \tag{2.2}$$

and for $N\Delta \leftrightarrow \Delta\Delta(\lambda=+1)$

$$\frac{1}{[\sqrt{p'^2+m_\Delta^2}-\sqrt{p^2+m_\Delta^2}]^2-q^2-\mu^2}\,. \tag{2.3}$$

B. Diagonal potentials

The diagonal potentials represent interactions for $NN \leftrightarrow NN$, $N\Delta \leftrightarrow N\Delta$, and $\Delta\Delta \leftrightarrow \Delta\Delta$. We will discuss each of these below, giving the results for one-meson exchange in all cases. We discuss the two-meson exchange only in the case of $NN \to NN$, since we are primarily interested in this channel. Two-meson exchange potentials for $\Delta\Delta \to \Delta\Delta$ and $N\Delta \to N\Delta$ follow from similar considerations.

1. Nucleon-nucleon potential

The NN potential is slightly different from what it was in Ref. [1]. The one-meson exchange piece of it is the same and is given in Fig. 3 (identical to Fig. 1 of Ref. [1]).

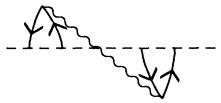

FIG. 3. One-meson-exchange folded diagram for the diagonal potential $NN \leftrightarrow NN$.

The time base for the nucleons is placed at the time midway between the absorption and emission vertices, again as in Ref. [1].

The two-meson-exchange processes consist of diagrams with NN intermediate states, $N\Delta$ intermediate states, and $\Delta\Delta$ intermediate states. Each of these has a two-meson-exchange box and a two-meson-exchange crossed box. The pieces with NN intermediate states are the same as before [1], and these are given in Fig. 4 (the same as Fig. 4 of Ref. [1]). There are two contributions, a true-correcting diagram [Fig. 4(a)] that must be added and a model-correcting diagram [Fig. 4(b)] that must be subtracted. The former arises because the two-meson exchanges cannot be built up from an iteration of the one-meson-exchange potential in Fig. 3, and the latter because iteration of Fig. 3 gives unwanted time orderings (the short-dashed lines are the time bases of the corresponding one-meson-exchange potentials).

The crossed box diagrams for $N\Delta$ and $\Delta\Delta$ intermediate states are also the same as before, given in Figs. 5(a) and 6(a), respectively (see Figs. 2(b) and 3(b) of Ref. [1]), but the corresponding two-meson exchange box diagrams are different, since these are now (partially) constituted from iterations of the $NN\leftrightarrow N\Delta$ and $NN\leftrightarrow\Delta\Delta$ transition potentials (including their Hermitian conjugates). Instead, we have a set of double-box diagrams shown in Figs. 5(b) and 6(b). The purpose of the double-box diagrams in Figs. 5 and 6 is analogous to what it was in Fig. 4, namely, to correct for under- and over-counting of the iteration of the $NN\leftrightarrow N\Delta$ and $NN\leftrightarrow\Delta\Delta$ transition potentials. The algebraic expressions corresponding to Figs. 3, 4, 5(a), and 6(a) are discussed in detail in Ref. [1]. The algebraic expression for the denominator in Fig. 6(b) is the same as Fig. 4(b), except that the mass of the appropriate intermediate nucleon in Fig. 4(b) should be replaced by the mass of the Δ to obtain the corresponding diagram in Fig. 6.

The different treatment of the double-box model-correcting folded diagrams in Figs. 5(b) and 6(b) is a consequence of the different choice of time base in the corresponding one-meson exchange contribution of the transition potential (for the former it was chosen at the meson-nucleon-delta vertex and for the latter midway between the emission and absorption vertices). Discussion

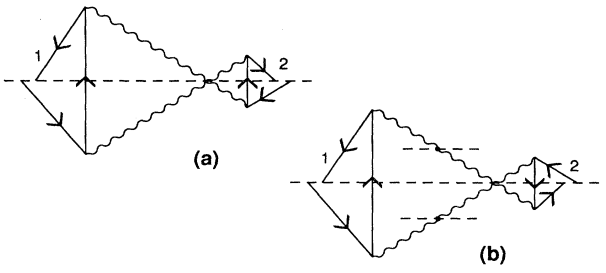

FIG. 4. Double-box two-meson-exchange folded diagrams: (a) a true-correcting double-box folded diagram, and (b) a model-correcting double-box folded diagram. Another model-correcting diagram exists for which the role of nucleons 1 and 2 is reversed.

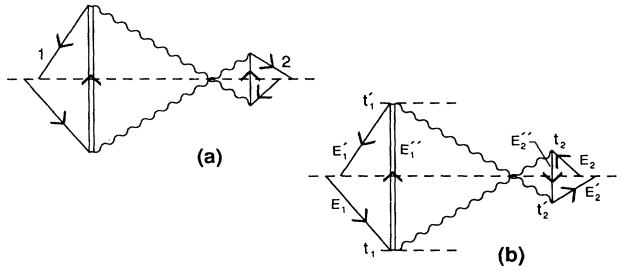

FIG. 5. Double-box two-meson-exchange folded diagrams: (a) is a true-correcting double-box folded diagram, and (b) is a model-correcting double-box folded diagram. Another set of diagrams exists for which the role of nucleons 1 and 2 is reversed.

of Figs. 5 and 6 along with explicit algebraic expressions for the denominator structure of Fig. 5(b) are found in Appendix A.

2. *Delta-delta potential*

The $\Delta\Delta$ potential is not used in the current treatment, but the folded diagrams for it are constructed in complete analogy to the NN potential, with the role of the N and Δ being exchanged everywhere. The one-meson-exchange potential is given in Fig. 7, and the denominator structure is the same as in Eq. (2.2).

3. *Nucleon-delta potential*

One should distinguish the direct and exchange contribution to the interaction. By direct (exchange) we mean that the Δ is on the same (opposite) nucleon line in the initial and the final state in the $N\Delta$ potential. These two cases must be treated differently in the potential. We consider only the one-meson-exchange potentials here, and these are discussed in Sec. B 3 a and B 3 b.

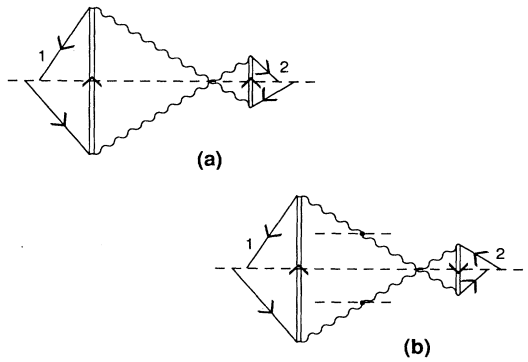

FIG. 6. Double-box two-meson-exchange folded diagrams: (a) is a true-correcting double-box folded diagram, and (b) is a model-correcting double-box folded diagram. Another model-correcting diagram exists for which the role of nucleons 1 and 2 is reversed.

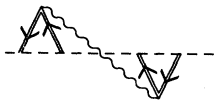

FIG. 7. One-meson-exchange folded diagram for the delta-delta interaction.

a. Direct one-meson exchange potential for $N\Delta$. The box for the direct one-meson-exchange potential is shown in Fig. 8(a). In this case, we choose the time base halfway between times t_1 and t_2, as shown in Fig. 9. We may then use Eq. (19) ($\lambda=0$) of Ref. [1] to obtain for the denominator

$$\frac{1}{[(\sqrt{p'^2+m_\Delta^2}-\sqrt{p^2+m_\Delta^2})-(\sqrt{p'^2+m_N^2}-\sqrt{p^2+m_N^2})]^2-q^2-\mu^2}\ . \tag{2.4}$$

In the case of equal mass baryons, this reduces to the usual "static" form used for the one-meson-exchange NN potential.

b. Exchange one-meson-exchange potential for $N\Delta$. The $N\Delta$ exchange diagram shown in Fig. 8(b) bears a very close relationship to the Δ self-energy shown in Fig. 8(c). For physical Δ, both have a singularity [Fig. 8(c) provides a width to the Δ, for example] and both need to be included in this case in order to be consistent with unitarity above pion production threshold. Because of the close connection between the two implied by unitarity, we believe that for consistency we should either include both or exclude both everywhere. Since we are not including the self-energy of the Δ explicitly for the present application, this means that we should also omit the $N\Delta$ one-meson-exchange potential in Fig. 8(b) in our current work. Above the threshold, both should be included.

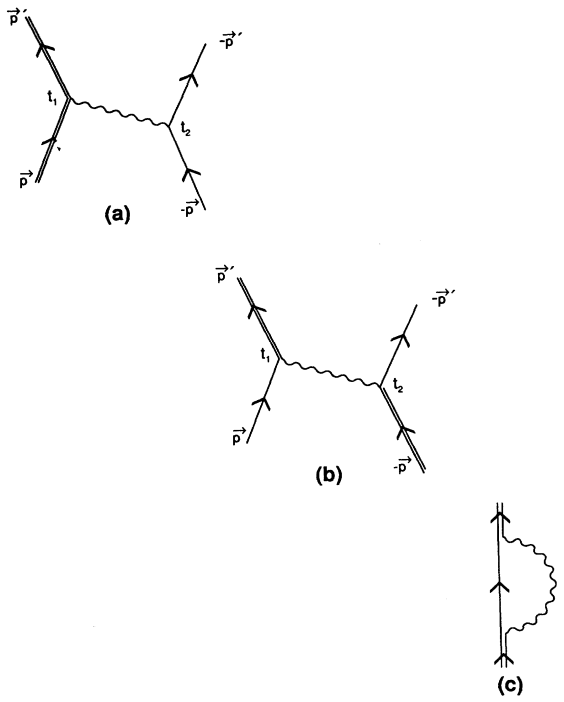

FIG. 8. One-meson-exchange boxes contributing to the direct (a) and exchange (b) $N\Delta$ potential, and (c) a contribution to the Δ self-energy.

III. CALCULATIONS

We show results here for the NN phase shifts, for the deuteron properties, and for nuclear-matter properties using the coupled-channel potential. These results are based on a particular selection of terms, consisting of the one-meson-exchange contributions to the transition potential for $NN\leftrightarrow N\Delta$ and $NN\leftrightarrow\Delta\Delta$, shown in Figs. 2(a) and 2(b), mediated by $\pi+\rho$ exchange. In addition, we retain the full NN potential shown in Fig. 3 for one-meson exchange ($\pi,\rho,\omega,\sigma',\delta$) and Figs. 4–6 for two-meson exchange, including ($\pi\pi,\pi\rho,\pi\sigma',\pi\omega$) for NN intermediate states and ($\pi\pi,\pi\rho$) for $N\Delta$ and $\Delta\Delta$ intermediate states subject to the approximations discussed in the Appendix. The analytic expressions for the meson-baryon vertex functions are taken to be precisely the same as in the full Bonn potential [3]. Although this model is far from complete, it is chosen as our first application because it is nearly identical to the single-channel folded diagram potential of Ref. [1]. The differences mainly occur in the more exact treatment of coupling to the $N\Delta$ (and $\Delta\Delta$) channel, which becomes increasingly important as the energy is raised toward pion-production threshold. Also, by virtue of our coupled-channel treatment, energy-dependent $\rho\rho$ contributions to the $N\Delta$ and $\Delta\Delta$ box diagrams are now automatically included (as for the NN case) whereas, in complete consistency with our treatment of the NN channel, the $\rho\rho$ contributions of the crossed-box and folded diagrams are omitted.

In order to obtain the NN scattering phase shifts, we have to solve for the scattering amplitude T, which in the folded-diagram expansion is given by

$$T(z)=V+V\frac{1}{z-h_0}T(z)\ , \tag{3.1}$$

acting now in the extended model space involving NN, $N\Delta$, and $\Delta\Delta$ intermediate states. The variable z is the two-nucleon (relativistic) starting energy and h_0 contains

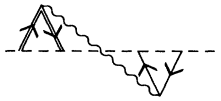

FIG. 9. One-meson-exchange folded diagram for the direct $N\Delta$ potential.

corresponding NN, $N\Delta$, and $\Delta\Delta$ intermediate states. Since in the present interaction model diagonal $N\Delta$ and $\Delta\Delta$ interactions are absent, the coupled-channel equation in Eq. (3.1) can be transformed into a simpler single-channel (NN) equation

$$T_{NN,NN}(z)=V^{\rm eff}_{NN,NN}(z)+V^{\rm eff}_{NN,NN}(z)\frac{1}{z-h_0^{(\rm NN)}}T_{NN,NN}(z)\ , \tag{3.2}$$

with

$$V^{\rm eff}_{NN,NN}(z)=V_{NN,NN}+\sum_{\alpha=N\Delta,\Delta\Delta}V_{NN,\alpha}\frac{1}{z-h_0^{\alpha}}V_{\alpha,NN}\ . \tag{3.3}$$

Corresponding equations hold for the deuteron wave function,

$$|\Psi(z_D)\rangle=\frac{1}{z_D-h_0}V|\Psi(z_D)\rangle \tag{3.4}$$

and

$$|\Psi_{NN}(z_D)\rangle=\frac{1}{z_D-h_0^{(NN)}}V^{\rm eff}_{NN,NN}(z_D)|\Psi_{NN}(z_D)\rangle\ . \tag{3.5}$$

The meson-nucleon coupling parameters (coupling constants, cutoff masses) obtained from a best fit to the empirical NN phase shifts, ($^1S_0$ and $^3S_1$) scattering lengths and the deuteron binding energy are shown in Table I and compared with those used in the full Bonn potential [3]. The corresponding phase shifts are given in Fig. 10, where one sees curves corresponding to the full Bonn potential [3] (dashed curve), the single-channel folded-diagram potential (FULLF, dash-dotted curve) [1], and the current coupled-channel potential (CCF, solid curve). As expected, the coupled-channel folded-diagram potential gives a substantially better description compared to the single-channel folded-diagram potential: There is a dramatic improvement in the $^1D_2$ partial wave, which is strongly coupled to the $N\Delta$ channel by the $\pi+\rho$ exchange $NN\leftrightarrow N\Delta$ transition potential. Also the important S waves are now perfectly reproduced. These improvements are made possible by the more exact treatment of the analytical structure (especially the energy dependence) of the scattering amplitude by the coupled-channel equations. For the other partial waves there is in some cases a slight improvement ($^3P_0, ^1P_1, ^3D_2$) and in others a slight worsening ($^3P_1, ^3D_1, ^3P_2$) of the results.

Although the description of our present model is surely sufficiently quantitative to allow for meaningful nuclear structure calculations, it still shows some deficiencies compared to that of the full Bonn potential, in some P waves as well as in $^3D_1$. To some extent, these can be traced to the ($N\Delta$ and $\Delta\Delta$) box diagrams involving 2ρ exchange, which are now automatically included due to the coupled-channel treatment but have been left out in the full Bonn potential. On the other hand, correlated $\pi\rho$ exchange is, so far, missing in both models and, for various reasons, should be included. It will be interesting to see whether this contribution will remove the current discrepancies.

Table II contains the results for the deuteron and low-energy parameters, for both the present (CCF) and the former (FULLF) folded-diagram model as well as for the full Bonn potential taken from Ref. [3]. In all cases the deuteron binding energy as well as both scattering lengths have been fitted, whereas all other quantities are predictions. The coupled-channel model leads to a $\Delta\Delta$ probability P_Δ of 1.36%, somewhat larger than the full Bonn potential. As in Ref. [3], we here ignore "renormalization" effects (for CCF and the Bonn potential) and calculate the deuteron properties from the nucleonic wave functions normalized to unity. As a consequence, in those cases the resulting values of A_S are somewhat larger than the experimental value. Note the appreciable improvement in the value of the singlet effective range r_s in the coupled-channel model CCF compared to FULLF,

TABLE I. Meson parameters applied in our coupled-channel folded-diagram interaction CCF. Numbers in parentheses denote corresponding values of the full Bonn potential (Ref. [3]), when different. The nucleon mass $m=0.938\,926$ GeV; the mass of the Δ isobar $=1.232$ GeV.

Vertex	$I(J^P)$ of meson	Meson mass m_α (GeV)	$g_\alpha^2/4\pi$; $[f_\alpha/g_\alpha]$	Cutoff mass Λ_α (GeV)	n_α
$NN\pi$	$1(0^-)$	0.138 03	14.4	1.5 (1.3)	1
$NN\rho$	$1(1^-)$	0.769	0.82[5.8] (0.84)([6.1])	1.4	1
$NN\omega$	$0(1^-)$	0.782 6	26.0 (20.0)	2.0 (1.5)	1
$NN\delta$	$1(0^+)$	0.983	2.7252 (2.8173)	2.0	1
$NN\sigma'$	$0(0^+)$	0.550	6.5413 (5.6893)	1.7	1
$N\Delta\pi$	$1(0^-)$	0.138 03	0.224	1.3 (1.2)	1
$N\Delta\rho$	$1(1^-)$	0.769	18.31 (20.45)	1.2 (1.4)	2

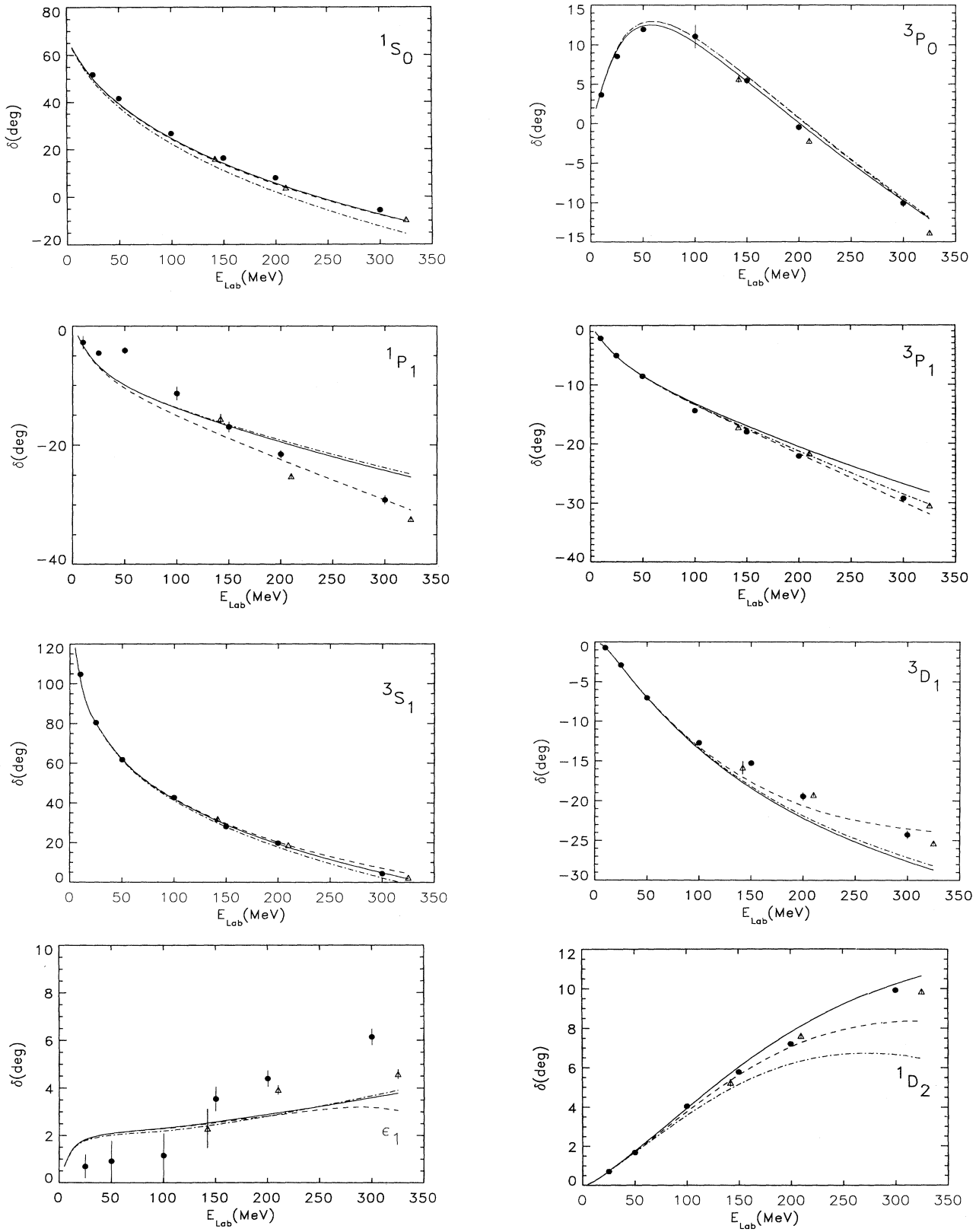

FIG. 10. Selected phase shifts for *n-p* scattering. The solid curve is the coupled-channel folded diagram-model (CCF) of this paper; the dash-dotted curve originates from the single-channel folded-diagram model (FULLF) of Ref. [1]; the dashed lines are from the full Bonn potential [3]. Experimental phase shifts are from the analysis of Arndt *et al.* [13] (solid circles) and Bugg [14] (triangles).

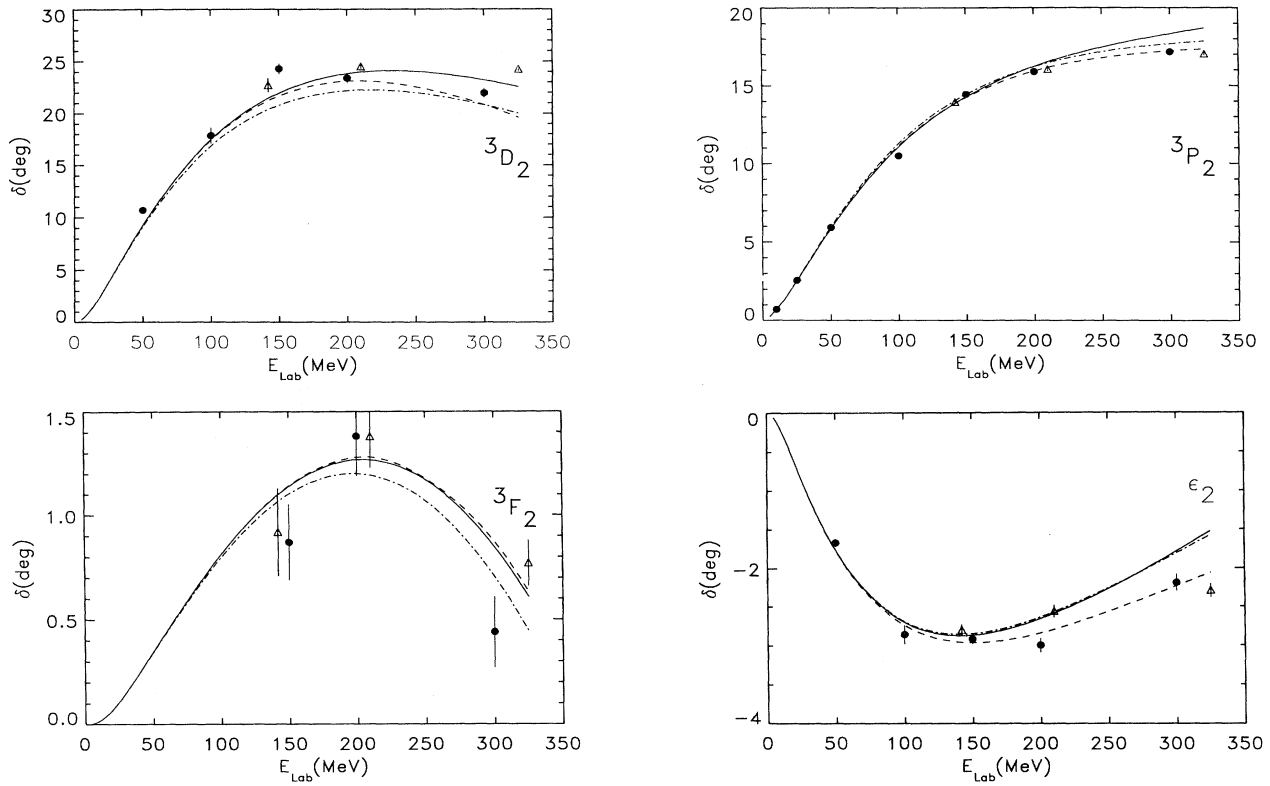

FIG. 10. (*Continued*).

which is, of course, connected to the improvement in the energy dependence of the $^1S_0$ phase shift discussed before.

As a first application of our coupled-channel model, we have calculated the binding energy E of infinite nuclear matter in lowest-order Brueckner theory. Then, E is given by (with m,n denoting occupied nucleon states)

$$E=\sum_m \langle m|h_0^{(NN)}|m\rangle + \frac{1}{2}\sum_{m,n}\langle mn|G_{NN,NN}(\omega)|mn-nm\rangle \ . \tag{3.6}$$

TABLE II. Deuteron and low-energy scattering parameters, predicted by our coupled-coupled folded-diagram potential CCF, by the single-channel model FULLF [1], and by the full Bonn potential [3], compared with experiment. Note that for CCF and the Bonn potential the deuteron properties are calculated from the nucleonic wave functions normalized to unity. The low-energy scattering data are from Dumbrajs *et al.* [19].

	CCF	FULLF	Full Bonn	Expt.
		Deuteron		
Binding energy (MeV)	2.2245	2.2244	2.2247	2.224 575[a]
P_d (%)	5.58	5.22	4.25	
Q_d (fm^2)	0.2852	0.2796	0.2807	0.2859±0.0003[b]
A_S (fm$^{-1/2}$)	0.8927	0.8866	0.9046	0.8846±0.0016[c]
Asymptotic D/S ratio	0.0267	0.0264	0.0267	0.0256±0.0004[d]
ΔΔ probability (%)	1.36	0.0	0.50	
	Neutron-proton low-energy scattering (scattering length a, effective range r)			
$^1S_0$: a_s (fm)	−23.75	−23.76	−23.75	−23.758±0.010
r_s (fm)	2.743	2.812	2.766	2.75±0.05
$^3S_1$: a_t (fm)	5.429	5.436	5.427	5.424±0.004
r_t (fm)	1.753	1.766	1.755	1.759±0.005

[a]Reference [15].
[b]Reference [16].
[c]Reference [17].
[d]Reference [18].

Here, the first term denotes the (relativistic) kinetic energy of the nucleons in the Fermi sea; the G matrix depends on the starting energy $\omega=\epsilon_m^{(N)}+\epsilon_n^{(N)}$ and is obtained from a solution of the Bethe-Goldstone equation

$$G(\omega)=V+V\frac{Q}{\omega-h}G(\omega) \tag{3.7}$$

acting in the extended model space. As usual Q denotes the Pauli projector and h describes the single-particle energies in intermediate states; it contains, in addition to the (relativistic) free-particle energies E_m, single-particle potentials building up the total single-particle energies ϵ_m. As before, the coupled-channel equation (3.7) can, in our case, be transformed into

$$G_{NN,NN}(\omega)=\bar{V}^{\text{eff}}_{NN,NN}(\omega)+\bar{V}^{\text{eff}}_{NN,NN}(\omega)\frac{Q^{(NN)}}{\omega-h^{(NN)}}G_{NN,NN}(\omega)\ , \tag{3.8}$$

with

$$\bar{V}^{\text{eff}}_{NN,NN}(\omega)=V_{NN,NN}+\sum_{\alpha=N\Delta,\Delta\Delta}V_{NN,\alpha}\frac{Q^{\alpha}}{\omega-h^{\alpha}}V_{\alpha,NN}\ . \tag{3.9}$$

A comparison of Eqs. (3.3) and (3.9) shows that the coupled-channel treatment leads to a modification of the (effective) NN interaction in the medium arising from the different propagator in the second term. Note, however, that in contrast to former treatments [5], the present scheme keeps $V_{NN,NN}$ as well as $V_{NN,\alpha}$ unmodified, making the present calculations much simpler than before.

In order to determine the single-particle energies ϵ_m we will use two alternative prescriptions. According to the "continuous" choice, the nucleon energies are fixed by

$$\epsilon_m^{(N)}=E_m^{(N)}+\sum_n\langle mn|G_{NN,NN}(\epsilon_m^{(N)}+\epsilon_n^{(N)})|mn-nm\rangle \tag{3.10}$$

for all momenta k_m, whereas the "standard" or "gap" choice uses this formula for occupied nucleon states ($k_m\le k_F$) only, and $\epsilon_m^{(N)}=E_m^{(N)}$ for $k_m\ge k_F$. In both cases, we take $\epsilon_m^{(\Delta)}=E_m^{\Delta}$, i.e., introduce no single-particle potential for the Δ. This is demanded by the gap choice and does not imply that the Δ does not interact with other nucleons.

According to Eq. (3.10), the G matrix has to be determined self-consistently. Figure 11 shows the resulting energy per particle, E/A, as a function of the Fermi momentum k_F, for both the continuous and the gap choice, for the present coupled-channel interaction model, in comparison to results obtained with our former single-channel interaction model (FULLF, Ref. [1]). Obviously, there is a strong repulsive effect, shifting the saturation points (E/A,k_F) from (−16.99 MeV, 1.55 fm^{-1}) to (−6.82 MeV, 1.07 fm^{-1}) for the continuous choice and from (−13.73 MeV, 1.55 fm^{-1}) to (−4.76 MeV, 1.07 fm^{-1}) for the standard choice. It is interesting to note that in both models the continuous choice leads to precisely the same saturation density as the standard choice, however, as expected, with a larger binding energy.

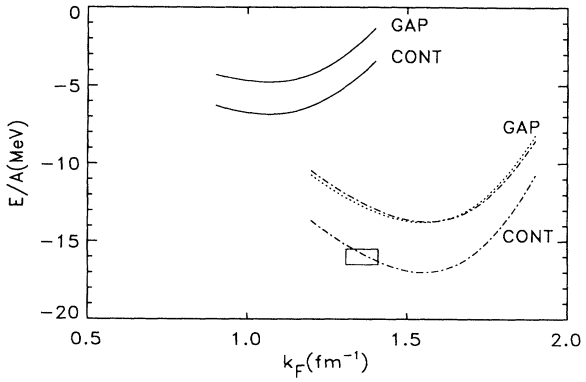

FIG. 11. Energy per nucleon of nuclear matter as a function of the Fermi momentum k_F, for both the continuous and gap choices of single-particle potential as defined in the text. The solid curves result from the present coupled-channel model (CCF), whereas the dash-dotted curves originate from the single-channel model (FULLF) of Ref. [1]. The dotted curve is obtained if Pauli and dispersive effects are switched off in CCF as described in the text. The small box represents the empirical saturation point.

If we switch off Pauli and dispersive effects in $\bar{V}^{\text{eff}}_{NN,NN}$ of our model CCF, i.e., replace $Q^{\alpha}/(\omega-h^{\alpha})$ by $1/(\omega-h_0^{\alpha})$ in Eq. (3.8) we obtain, based on the gap choice, an almost identical result for the binding energy as with FULLF, as expected. This is not only true for the total result but (to a slightly lesser extent) also for the single partial wave contributions [cf., CCF (NDE) and

TABLE III. Partial-wave contributions (in MeV) to the binding energy of nuclear matter, E/A, for our coupled-channel folded-diagram potential CCF and for FULLF (Ref. [1]) at $k_F=1.5$ fm^{-1}. CCF (NDE) denotes the results when Pauli and dispersive effects are switched off in CCF, as explained in the text.

	CCF	CCF (NDE)	FULLF
$^1S_0$	−12.52	−20.44	−19.81
$^3P_0$	−4.02	−4.43	−4.67
$^1P_1$	5.56	5.57	5.47
$^3P_1$	16.68	14.90	14.93
$^3S_1$	−19.53	−20.72	−21.28
$^3D_1$	2.39	2.39	2.38
$^1D_2$	−3.43	−4.05	−3.83
$^3D_2$	−5.82	−5.81	−5.74
$^3P_2$	−7.27	−10.36	−10.35
$^3F_2$	−0.88	−0.91	−0.90
$J=3$	4.40	4.44	4.46
$J=4$	−2.52	−2.52	−2.50
$5\le J\le 12$	0.75	0.75	0.76
Potential energy	−26.21	−41.19	−41.09
Kinetic energy	27.51	27.51	27.51
E/A	1.30	−13.68	−13.58

FULLF in Table III]. Slight discrepancies, which happen to essentially cancel in the total sum for the potential energy, can, in general, be traced to differences in the corresponding NN scattering phase shifts between CCF and FULLF. Table III also shows that the dominant shift occurs in isospin-1 states ($^1S_0, ^3P_1, ^3P_2, \ldots$) and is therefore mainly generated by both Pauli and dispersive effects on the $N\Delta$ (and ΔN) states.

IV. DISCUSSION

A coupled-channel approach in which delta and nucleon degrees of freedom are treated on an equal footing is useful for a variety of reasons. On the one hand, it facilitates the study of the interplay between the Δ and N degrees of freedom and the bound-state properties of nuclear matter and nuclei. Secondly, it provides a natural framework for extending models that have been successful for studies of the NN interaction to the case of the $N\Delta$ and $\Delta\Delta$ interaction. Such extensions are important, for example, because of the significant role played by the $N\Delta$ interaction in pion-nucleus scattering [6]. Finally, for future quantitative studies of NN scattering above the pion-production threshold, a coupled-channel description with NN, $N\Delta$, and $\Delta\Delta$ channels is likely to be required.

In this work we have looked at the calculation of the interaction for such a coupled-channel approach within the framework of folded diagrams and meson theory. Folded diagrams provide a means to calculate an energy-dependent (but nonlocal) interaction equivalent to the underlying meson-exchange interaction. We have chosen the folded-diagram description because energy-independent interactions are generally easier to work with than energy-dependent ones. We have found that we can consistently define an energy-independent interaction using folded diagrams, and we have given explicit expressions for these cases.

For the numerical results in this paper, we have been interested only in the NN channel. We have therefore restricted the selection of diagrams that make up the coupled-channel potential as described in Sec. III. For future applications, a more complete selection should be considered. For example, a realistic description of the $N\Delta$ interaction (not considered in this paper) might require inclusion of not only one- but also two-meson-exchange pieces of the diagonal potential in this sector. Future studies can also show whether the diagonal $\Delta\Delta$ potential and the pieces of the transition potentials involving two (and more) meson exchange, which have also been omitted in this work, play an important role in the NN problem.

Bearing in mind our limited application of the coupled-channel approach in this paper, our numerical studies show nevertheless encouraging results. We have found that the more exact treatment of the $N\Delta$ threshold improves the overall agreement with the NN phase shifts compared to the single-channel model [1]. Slight discrepancies still remain, which might disappear if the physics of the model is enlarged by including, e.g., correlated $\pi\rho$ exchange. However, as a model constructed for application in nuclei and nuclear matter, the present small differences at higher energies are irrelevant, as shown in Ref. [1].

Apart from applications in nuclear matter, this model should be especially useful for applications in the triton. Several interesting results have been obtained recently for this system based on alternative coupled-channel models constructed by the Hannover [7] and Argonne [8] groups. (The NN part of the first model is based on the Paris potential [9].) For both models, Picklesimer, Rice, and Brandenburg [10] have found that repulsive Δ dispersive effects and attractive three-body force effects tend to cancel in the trition binding energy. Furthermore, quantitative calculations require that not only the one-Δ but also $\Delta\Delta$ components are taken into account. However, these authors also point out that, since $\Delta\Delta$ effects turn out to be large, $\Delta\Delta\Delta$ contributions have to be examined, too, and since there are no $\Delta\Delta\Delta$ dispersive effects, any $\Delta\Delta\Delta$ three-body force contribution translates directly into an increase in the triton binding energy. Moreover, Stadler and Sauer [11] have found using the Hannover model [7] that the irreducible part of the Tucson-Melborne three-body force [12] not mediated by Δ-excitation makes a non-negligible contribution to the triton binding energy.

Compared to the interaction models [7,8], our model differs in various aspects. First, it is based on nonlocal meson-baryon vertex functions obtained from field theory; the only parameters are coupling constants and cutoff masses chosen consistently in the NN and $N\Delta$ sectors. Secondly, it includes higher-order diagrams, which correct for the restrictions to instantaneous interactions of lowest order, to the level of the full Bonn potential [3], with the advantage of a simpler application in nuclear structure. It would be interesting to see if the conclusions obtained by the authors of Refs. [10,11] essentially survive if the coupled-channel model presented in this paper is applied. In any case, some increase of the triton binding energy is expected from the nucleons—only part, since (i) the deuteron D-state probability, due to the nonlocal structure of the interaction, is somewhat lower in models [7,8], and (ii) our model is fitted to the n-p data. This is suggested already from the (five-channel) evaluation [1] based on the single-channel folded-diagram model (FULLF) yielding a triton binding of 7.86 MeV, compared to 7.3 MeV for the Paris [9] and 7.44 MeV for the Argonne V14 models [8], respectively, obtained with the same restrictions in the NN input.

ACKNOWLEDGMENTS

This work was supported in part by the Deutsche Forschungsgemeinschaft Az. Schu 439/7-1 and the U.S. Department of Energy, Contract W-7405-ENG-36. M.B.J. acknowledges the financial support of the Humboldt Foundation and the generous hospitality of the Theory group of Jülich.

APPENDIX

1. Evaluation of Fig. 5(b)

As in Ref. [4], we write the value of the folded diagram in Fig. 5(b) as a vertex contribution (taken from the Bonn potential [3]) and a propagator contribution, $J^{5(b)}$. The propagator contribution consists of an internal part, $W^{5(b)}(t_1't_1t_2't_2)$, and a part for the external nucleon lines. The rules for evaluating the diagram are the same as those given in Sec. III of Ref. [4]. The function $W^{5(b)}$ may be written in the form

$$W^{5(b)}(t_1't_1t_2't_2)=\left[\frac{1}{2\pi}\right]^4\int d\nu_1'd\nu_1d\nu_2'd\nu_2 e^{-it_1'\nu_1'}e^{-it_1\nu_1}e^{-it_2'\nu_2'}e^{-it_2\nu_2}(2\pi)\delta(\nu_1'+\nu_1+\nu_2'+\nu_2)w^{5(b)}(\nu_1'\nu_1\nu_2'\nu_2)\ , \tag{A1}$$

where the delta-function expresses invariance with respect to time-translations. The external legs in each case contribute

$$e^{-iE_1'(t_0-t_1)}e^{-iE_1(t_1-t_0)}e^{-iE_2'(t_0-t_2)}e^{-iE_2(t_2-t_0)}\ , \tag{A2}$$

where t_0 is the time-base of Fig. 5(b). The time base is fixed at the average time $(t_1'+t_1+t_2'+t_2)/4$. The evaluation for $J^{5(b)}$ is found by integrating over all times subject to this constraint. We then have, following the straightforward calculation similar to that in Appendix B of Ref. [4],

$$J^{5(b)}=iw^{5(b)}(\bar{E},-\bar{E},\bar{E},-\bar{E})\ , \tag{A3}$$

where

$$\bar{E}=(E_1+E_1')/2=(E_2+E_2')/2\ . \tag{A4}$$

It now remains to calculate $w^{5(b)}(\nu_1',\nu_1,\nu_2',\nu_2)$. The ingredients are the internal nucleon, the meson propagators, and the time constraints that maintain the proper time orderings of the time bases represented by the horizontal dashed lines in Fig. 5(b). The meson propagators are

$$(1/2\pi)\int_{-\infty}^{+\infty}d\omega[e^{-i\omega\Delta t}/(\omega^2-e_q^2+i\eta)]\ , \tag{A5}$$

where $e_q=(q^2+\mu^2)^{1/2}$ is the energy of a meson, and the nucleon propagator is given by

$$e^{-iE_k\Delta t}\theta(\Delta t)=(1/2\pi)\int_{-\infty}^{+\infty}d\omega[e^{-i\omega\Delta t}/(\omega-E_k+i\eta)]\ . \tag{A6}$$

Putting together the various propagators and time restrictions, we find

$$W^{5(b)}(t_1't_1t_2't_2)=\left[\frac{i}{2\pi}\right]^4\int d\omega_1d\omega_2d\omega_3d\omega_4\frac{e^{-i\omega_1(t_1'-t_1')}}{\omega_1-E_1''+i\eta}\frac{e^{-i\omega_2(t_2-t_2')}}{\omega_2-E_2''+i\eta}\frac{e^{-i\omega_3(t_2-t_1)}}{\omega_3^2-e_3^2-i\eta}\frac{e^{-i\omega_4(t_2'-t_1')}}{\omega_4^2-e_4^2+i\eta}\ . \tag{A7}$$

If we now change variables in Eq. (A7) as follows,

$$\begin{aligned}\nu_1'&=\omega_1-\omega_4\ ,\\ \nu_1&=-\omega_1-\omega_3\ ,\\ \nu_2'&=-\omega_2+\omega_4\ ,\\ \nu_2&=\omega_2+\omega_3\ ,\end{aligned} \tag{A8}$$

then we find Eq. (A1) to hold with

$$w^{5(b)}(\nu_1'\nu_1\nu_2'\nu_2)=-\int\frac{d\omega}{2\pi}\frac{1}{(\nu_1'+\omega-E_1''+i\eta}\frac{1}{-\nu_2'+\omega+E_2''-i\eta}\frac{1}{(\nu_1'+\nu_1+\omega)^2-e_3^2+i\eta}\frac{1}{\omega^2-e_4^2+i\eta}\ . \tag{A9}$$

We next evaluate Eq. (A9) by closing the contour in the upper 1/2 plane. Thus, we find

$$\begin{aligned}J^{5(b)}=\frac{1}{4e_3e_4}\Bigg\{&\frac{1}{2\bar{E}-E_1''-E_2''}\left[\frac{1}{\bar{E}-E_1''-e_3}\frac{1}{\bar{E}+E_1''-e_4}-\frac{1}{\bar{E}-E_2''+e_3}\frac{1}{-\bar{E}-E_2''+e_4}\right]\\ &-\frac{1}{e_3+e_4}\left[\frac{1}{\bar{E}-E_1''-e_3}\frac{1}{\bar{E}-E_2''+e_3}+\frac{1}{\bar{E}-E_1''-e_4}\frac{1}{\bar{E}-E_2''+e_4}\right]\Bigg\}\ .\end{aligned} \tag{A10}$$

2. Approximations

Several approximations have been made when evaluating the diagrams of Figs. 5 and 6.

Concerning the model-correcting diagrams of Fig. 5(b), we have replaced $2\bar{E}$ by $2m_N$ in order to avoid an apparently (in comparison to the Bonn potential) unrealistic off-shell behavior of the folded-diagram interactions. This was already done in Ref. [1], for the iterative folded diagram with $N\Delta$ and $\Delta\Delta$ intermediate states. As pointed out there, the occurrence of this off-shell behavior indicates that the energy dependence of the $N\Delta$ box is not capable of being described completely by a folded diagram. Note that in the present case this approximation is of much less relevance, since the major contribution of the $N\Delta$ box is now generated, with its correct energy dependence, by the iteration of the $N\Delta$ transition potential.

Since, for $N\Delta$ and $\Delta\Delta$ intermediate states, the iterative structure is excessively complicated for $\pi\rho$ exchange, the following approximations have been made, in analogy to Refs. [1,3]: First, in the model-correcting diagrams 5(b) and 6(b), the noniterative contributions have been omitted for $\pi\rho$ exchange; in other words, only the iterative part [first term in Eq. (A10)] has been kept (with the approximation described in the foregoing paragraph). Fortunately, it is the dominant contribution.

Concerning the true-correcting (crossed-box) diagrams of 5(a) and 6(a), we made an analogous approximation as in Refs. [1,3], replacing these diagrams by the values of the $\pi\rho$ folded box diagrams as evaluated in Figs. 2(a) and 3(a) of Ref. [1], with, however, the correct isospin factor, i.e., reversing the sign of the isospin-dependent $\tau_1\cdot\tau_2$ piece. As this procedure strongly overestimates the role of $N\Delta$ contributions in the ${}^3S_1-{}^3D_1$ channel (see Ref. [3]), we follow the procedure of Ref. [3] and omit this term in this channel.

Furthermore, as in Ref. [1], singularities in various propagators have been avoided by replacing E_q by $E_{q'}$ and vice versa (see the discussion in connection with Eq. (2.5) of Ref. [1]).

[1] J. Haidenbauer, K. Holinde, and M. B. Johnson, Phys. Rev. C **45**, 2055 (1992).

[2] M. B. Johnson, J. Haidenbauer, and K. Holinde, Phys. Rev. C **42**, 1878 (1990).

[3] R. Machleidt, K. Holinde, and Ch. Elster, Phys. Rep. **149**, 1 (1987).

[4] M. B. Johnson, Ann. Phys. (N.Y.) **97**, 400 (1976).

[5] M. R. Anastasio, A. Faessler, H. Müther, K. Holinde, and R. Machleidt, Phys. Rev. C **18**, 2416 (1978).

[6] M. B. Johnson and D. J. Ernst, Ann. Phys. (N.Y.) **219**, 266 (1992).

[7] Ch. Hajduk, P. U. Sauer, and W. Struewe, Nucl. Phys. **A405**, 581 (1983); Ch. Hajduk, P. U. Sauer, and S. N. Yang, Nucl. Phys. **A405**, 605 (1983).

[8] R. B. Wiringa, R. A. Smith, and T. L. Ainsworth, Phys. Rev. C **29**, 1207 (1984).

[9] M. Lacombe, B. Loiseau, J. M. Richard, R. Vinh Mau, J. Côte, P. Pirès, and R. de Tourreil, Phys. Rev. C **21**, 861 (1980).

[10] A. Picklesimer, R. A. Rice, and R. Brandenburg, Phys. Rev. Lett. **68**, 1484 (1992).

[11] A. Stadler and P. U. Sauer, Phys. Rev. C **46**, 64 (1992).

[12] S. A. Coon, M. D. Scadron, P. C. McNamee, B. R. Barrett, D. W. E. Blatt, and B. H. J. McKellar, Nucl. Phys. **A317**, 242 (1979).

[13] R. A. Arndt, J. S. Hyslop III, and L. D. Roper, Phys. Rev. D **35**, 128 (1987).

[14] D. V. Bugg, Phys. Rev. C **41**, 2708 (1990).

[15] C. van der Leun and C. Alderliesten, Nucl. Phys. **A380**, 261 (1982).

[16] D. M. Bishop and L. M. Cheung, Phys. Rev. A **20**, 381 (1979).

[17] T. E. O. Ericson and M. Rosa-Clot, Nucl. Phys. **A405**, 497 (1983); T. E. O. Ericson, *ibid.* **A416**, 281c (1984).

[18] N. L. Rodning and L. D. Knutsen, Phys. Rev. C **41**, 898 (1990).

[19] O. Dumbrajs *et al.*, Nucl. Phys. **B216**, 277 (1983).